

# JET PROPULSION OF WIND EJECTA FROM A MAJOR FLARE IN THE BLACK HOLE MICROQUASAR SS433

KATHERINE M. BLUNDELL<sup>1</sup> AND PAUL HIRST<sup>2</sup>

*Accepted by ApJ Lett*

## ABSTRACT

We present direct evidence, from Adaptive-Optics near-infra-red imaging, of the jets in the Galactic microquasar SS433 interacting with enhanced wind-outflow off the accretion disc that surrounds the black hole in this system. Radiant quantities of gas are transported significant distances away from the black hole approximately perpendicular to the accretion disc from which the wind emanates. We suggest that the material that comprised the resulting “bow-tie” structure is associated with a major flare that the system exhibited ten months prior to the observations. During this flare, excess matter was expelled by the accretion disc as an enhanced wind, which in turn is “snow-ploughed”, or propelled, out by the much faster jets that move at approximately a quarter of the speed of light. Successive instances of such bow-ties may be responsible for the large-scale X-ray cones observed across the W50 nebula by ROSAT.

*Subject headings:* Stars: Binaries: Close, Stars: Individual: SS433

## 1. INTRODUCTION

Although black holes are popularly thought of as simply sucking matter towards them, the astrophysical reality is rather different: energetic jets of matter are ejected in opposite directions away from near black holes, sometimes emitting as they do so via e.g. synchrotron radiation (Begelman et al. 1984). Gravitational attraction of matter occurs simultaneously with angular momentum conservation leading to matter swirling inwards in a plane and forming structures known as accretion discs. As well as jets, these discs themselves give rise to mass outflow via slow (non-relativistic) winds (Kuncic & Bicknell 2007), along approximately polar directions to the instantaneous plane of the accretion disc as it precesses (Perez & Blundell 2010; Blundell et al. 2008). The importance of mass outflow and energy outflow from black holes is being increasingly recognised as offsetting cooling and hence playing an important role in influencing the formation of cosmic structure by quasars and active galaxies but the details are little known and poorly understood to date (Bower et al. 2008; Cavaliere & Lapi 2008). Here we present direct evidence for the relativistic ( $0.2c - 0.3c$ ) jets in the microquasar SS433 propelling gas out to significant distances, in excess of a few light months, from its  $20 M_{\odot}$  black hole (Blundell et al. 2008), in a manner akin to how a snowplough moves snow. The gas propelled by the jets originates in the much slower wind from the accretion disc, for reasons explored in the following sections.

## 2. OBSERVATIONS AND DATA PROCESSING

Observations were carried out using the NACO (Rousset et al. 2003; Lenzen et al. 2003) instrument at the Nasmyth B focus of ESO’s VLT-UT4 telescope, employing the Ks-filter (centred at  $2.2 \mu\text{m}$  which includes the rest-frame Brackett- $\gamma$  at  $2.17 \mu\text{m}$ ) and S13 cam-

era giving a pixel scale of 13mas and field-of-view of 13arcsec. The standard technique of jittering the telescope position between exposures within a 5-arcsec box centred on the position of the SS433 nucleus was employed. Short exposure times ( $< 0.6$  seconds) were used to avoid saturating the detector pixels covering the bright SS433 nucleus. The Adaptive Optics (AO) system was employed with the visible-light wave-front sensor using the SS433 nucleus itself as the reference object. The resulting data files were inspected, and frames with obvious defects (arising from e.g. the AO loop opening, or excessive image elongation) were rejected. 487 frames, totalling 4287 seconds of exposure time remained.

Both 0.4 and 0.5-second exposure frames were obtained with NACO on 2005-08-18, co-added in groups of 20 by the data acquisition system. Initial data processing comprised dark correction (using the average of dark frames taken the following day, and having the same array configuration and exposure time as the science observations) and flat-field correction (using the average of the difference between lamp-on and lamp-off daytime observations of a flat-field calibration lamp in the same filter and array configuration as the science frames). Bad pixels were flagged in both the dark and flat-field images using a simple threshold to detect unphysical values. Following the processing of individual data-frames, a novel processing technique was used to form a clipped-mean stack image. This deep-stack image is dominated by the bright central nucleus of SS433, with the wings of this PSF spreading out over most of the image. To subtract the PSF, we constructed an azimuthally-averaged radial profile, centred on the nucleus, and including only those azimuthal ranges apparently devoid of structure. This radial profile was then azimuthally swept out to form a circularly-symmetric, model PSF image that was then subtracted from the deep-stack image data to yield a PSF-subtracted stacked image. This PSF subtraction does not model the detailed (non-circularly symmetric) structure close to the core of the PSF well, and thus this area has been masked out with 2.2-arcsecond diameter

<sup>1</sup> University of Oxford, Department of Physics, Keble Road, Oxford, OX1 3RH, U.K.

<sup>2</sup> Gemini Observatory, 670 North A‘ohōkū Place, University Park, Hilo, HI 96720, U.S.A.

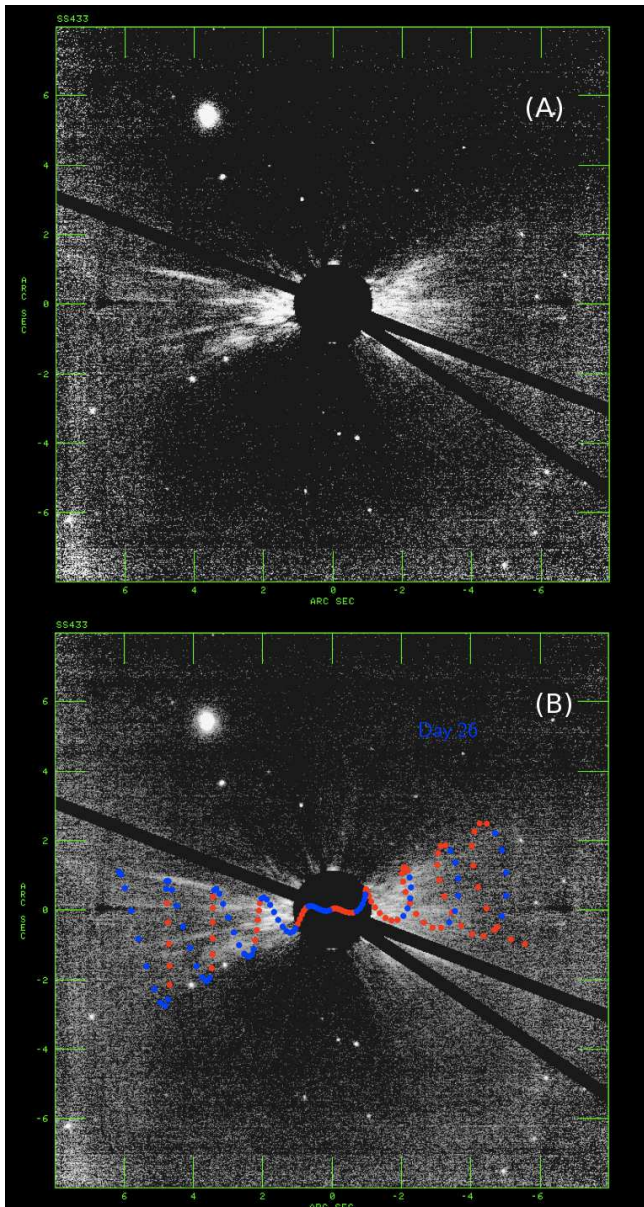


FIG. 1.— Adaptive-optics imaging from VLT-NACO of the microquasar SS433 located within our Galaxy at a distance of 5.5 kpc from Earth (Blundell & Bowler 2004; Lockman et al. 2007). Masking in black has been applied to the central region (within which azimuthal fidelity cannot be relied upon) and also to a diffraction spike and filter scratch as described in Sec 2. The lower panel has overlaid coloured dots delineating the location of successively launched jet bolides appropriate to the precession phase of the infra-red observation (assuming the kinematic model is obeyed exactly); those moving towards us are coloured blue and those moving away from us are coloured red. The correspondence of these with the infra-red emission on the east (left) side especially is remarkable. N.B. the two point sources on the south edge of the east cone projection are believed to be foreground sources, but radial streaks seen clearly on the eastern side mimic projected paths that the ballistically travelling bolides take.

circular mask. Two other apparent artefacts in the image have also been masked, believed to result from defects on the filter in use during the observations.

The individual data frames are dominated by the bright, unresolved central nucleus of SS433. Imaging artefacts apparent in each frame include 1) Bad pix-

els, with data values in either the science or calibration frames that are inconsistent with being due to incident light on the array, 2) electronic ghost images of the bright SS433 nucleus, “reflected” into the other array quadrants, caused by electronic cross talk, and 3) diffraction spikes radiating outwards from the bright SS433 nucleus, due to the presence in the telescope pupil of the vanes that support the secondary mirror unit of the telescope. In successive frames, the position angle of these diffraction spikes rotates in each successive frame with respect to the sky consistently with the parallactic angle of the observations (because the azimuth-elevation mount of the telescope means that the telescope pupil rotates with respect to the sky as the telescope tracks the target during observations). The next stage of data reduction was to flag pixels affected by these artefacts as bad so as to exclude them from subsequent processing. The exact position of the SS433 nucleus in the image was determined via a 2-d Gaussian fit at the expected position (inferred on the basis of information recorded in the header of each image) and exact alignment was then possible. The cross-talk artefacts were then masked with 50 by 10 pixel bad pixel blocks centred at the SS433 position reflected about the central pixel of the array. To mask the diffraction spikes, the angular offset of the artefacts relative to the telescope parallactic angle was determined empirically, and two bands of pixels centred on the SS433 nucleus and 14 pixels wide running across the entire image at the appropriate angles were flagged as bad. A clipped-mean stack from the large number of (short exposure) data frames was performed as follows: a data-cube was formed from the aligned frames, such that each ( $z$ ) plane of the cube consists of a single data frame, with the SS433 nucleus centred in the ( $x, y$ ) plane. The array of values over  $z$  at any given ( $x, y$ ) co-ordinate in the cube thus represents all our measurements of the flux from that particular point on the sky.

We next looped through each ( $x, y$ ) point, taking the array of values over  $z$  and sorting them by value in the cube, such that extreme values for any given point on the sky would “float up” or “sink down” close to the edges of the cube. We visually inspected the resulting cube to determine the number of planes to reject at both ends of the  $z$  axis to exclude outliers, rejecting 5 planes from the top of the cube and 2 from the bottom. The remaining planes of the cube were collapsed over the  $z$ -axis using an arithmetic mean to generate the deep-stack image. In forming the mean, we ensured pixels previously masked as bad in the individual frame processing were excluded.

Fig 1A shows an infra-red image taken with NACO, revealing a remarkable extended structure that approximately resembles a bow tie in appearance. Fig 1B shows that this structures reflects the projection of the cone traced out by the precession of the launch axis of its jets (Hjellming & Johnston 1981; Blundell & Bowler 2004). Importantly, the extent (over a few arcseconds) of the bow-tie structure goes way beyond the regime within a few PSFs (tenths of arcseconds) of the central star beyond where planet hunting via AO techniques is normally restricted (e.g. Lagrange et al. 2009). The bow-tie structure does not resemble any typical AO artefacts either in its azimuthal dependence or its radial extent (e.g. Gladysz & Christou 2009). To determine if any of the structure could be due to a transient artefact, the data



were re-stacked, split over time into four equally-sized chunks, and each chunk processed separately through the stacking and PSF-subtraction methods described. The bow-tie structure is clearly visible in each of the separate chunks, indicating that it is not an artefact correlated with parallactic angle or other rotational variable.

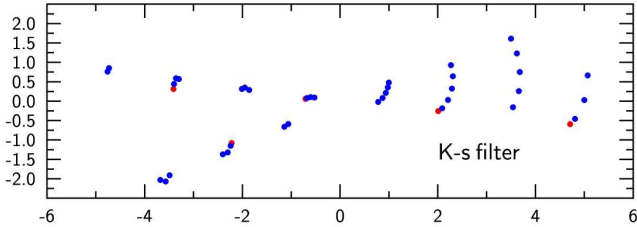


FIG. 2.— Spectral-filtering figure. This figure shows a prediction for the observed distribution of Brackett- $\gamma$  if the emitting material is launched in a way that exactly obeys the standard kinematic model for the precession of SS433’s jet axis (Hjellming & Johnston 1981). This illustration allows for the fact that material moving an inappropriate angle to our line-of-sight will be too redshifted or too blueshifted to give Brackett- $\gamma$  radiation within the Ks-band filter profile, whose lower and upper cut-offs are taken to be  $2.05 \mu\text{m}$  and  $2.27 \mu\text{m}$ .

### 3. EMISSION MECHANISM

We now consider what is the mechanism responsible for the bow-tie emission in the near-IR Ks-band shown in Fig 1, and whether there is any evidence that the radiating material is moving.

One possibility is that the structure is an ionisation cone similar that observed in LMC-X1 (Cooke et al. 2008) but this model would predict a brightness distribution symmetric on both sides of the nucleus, and marked east-west asymmetries are observed as examined in Sec 4. Producing the observed structure through the emission of Bremsstrahlung radiation would require a somewhat contrived density and temperature profiles, so line emission from the Brackett- $\gamma$  transition seems to be a more likely explanation. A definitive demonstration of Brackett- $\gamma$  emission from fast-moving material would be the detection of specific asymmetric brightness structures. For example, if the emitting material were moving at speed  $0.26c$  radially and ballistically away from the nucleus along the outside of the precession cone well known from radio imaging to be traced by the jet axis, and if it were radiating Brackett- $\gamma$  emission then the Ks-filter’s transmission profile through which the object is observed will act as a velocity filter because the different angles to the line-of-sight around the cone will cause the line emission to redshift and blueshift in and out of the filter profile. Fig 2 predicts the observed brightness distribution in this scenario and we note that qualitatively the west wing being more *filled in* and the east wing being more *edge brightened* reflects the actual observations shown in Fig 1: only radiation from material that is not too redshifted or too blueshifted will be observable. We contend that this asymmetric east-west appearance constitutes circumstantial evidence that the speed with which the emitting material is moving is close to  $0.26c$  and that the radiation mechanism is line emission from the Brackett- $\gamma$  transition.

### 4. PROPULSION MECHANISM

If material is travelling ballistically at around the speed of a quarter of the speed of light (i.e. the jet speed), then it will have left the nucleus at most 10-12 months previously (material travelling at the sorts of speeds associated with the poloidal disc wind in this object which is  $\sim 1000 \text{ km/s}$  would have travelled only a mere one third of an arcsec in this time). Ten months before the NACO observation depicted in Fig 1, i.e. on 2004 October 15, SS433’s central engine exhibited a major flare (Blundell et al. 2011) involving many physical phenomena: a spectacular increase in the intensity and speed of the accretion disc wind and a spectacular increase in the intensity and launch speed of the jet material, as well as subsequent flaring at radio wavelengths. During this flare the intensity of the disc wind, measured from the stationary hydrogen lines, more than doubled and the speed of the disc wind more than doubled to  $1300 \text{ km/s}$  (Blundell et al. 2011). The disc wind is known from spectroscopy (Perez & Blundell 2010; Blundell et al. 2008) to be poloidal and thus approximately aligned along the cone of the jet axis. Matter ejected as part of the enhanced disc wind during that flare, and propelled with the same range of speeds that the jet material is observed to move at (namely a range spanning  $0.2c$  to  $0.3c$  — (see fig 2c of Blundell & Bowler 2005)) and travelling ballistically as the jet material does, will be distributed along the same radial paths from SS433’s nucleus as the emission seen in Figure 1A, if launched with the same angular distribution as the jet bolides (Fig 1B). Note that the stochastic variations in speed and in direction of the jets (Blundell, Bowler & Schmidtobreich 2007) will blur out the gas distribution further. Thus, remarkably, it would appear that the jets (well known to move at these speeds) sweep up and propel this “cloud” of gas that was ejected as disc wind during the flare, out to much larger distances by the time of our NACO observation than would otherwise be the case if moving at speeds of merely  $\sim 1000 \text{ km/s}$ . We suggest this process is what gives rise to the radial streaks (“ionisation trails”) observed most clearly on the left hand side in Fig 1. There would be no discernible deceleration of the jet as long as the ram pressure of the jet bolides is sufficiently large (which translates to the condition that the density through which the bolides propagate is less than  $\sim 10^{-21} \text{ kg m}^{-3}$  (assuming the density of the line-emitting bolides inferred by Panferov & Fabrika (1997), their size from Mioduszewski et al. (2004), and expansion rate from Blundell, Bowler & Schmidtobreich (2007), and noting that the propagation of the jet bolides remains ballistic over many light-months; the simulations of Goodall et al. (2011) suggest a density of  $3 \times 10^{-22} \text{ kg m}^{-3}$  consistent with this picture). There was a subsequent single epoch at which this system was observed with adaptive optics imaging at Ks-band, 2009 April 24, and at most only hints of a bow-tie structure were detected on this occasion, although conditions were remarkably poor for AO observing ( $1.6''$ ) seeing. There was no major flare that preceded this epoch at an appropriate interval that would have given rise to the bow-tie structure seen at the first epoch. We conclude that the bow tie is a transient structure only present after the central engine of this microquasar has exhibited a ma-

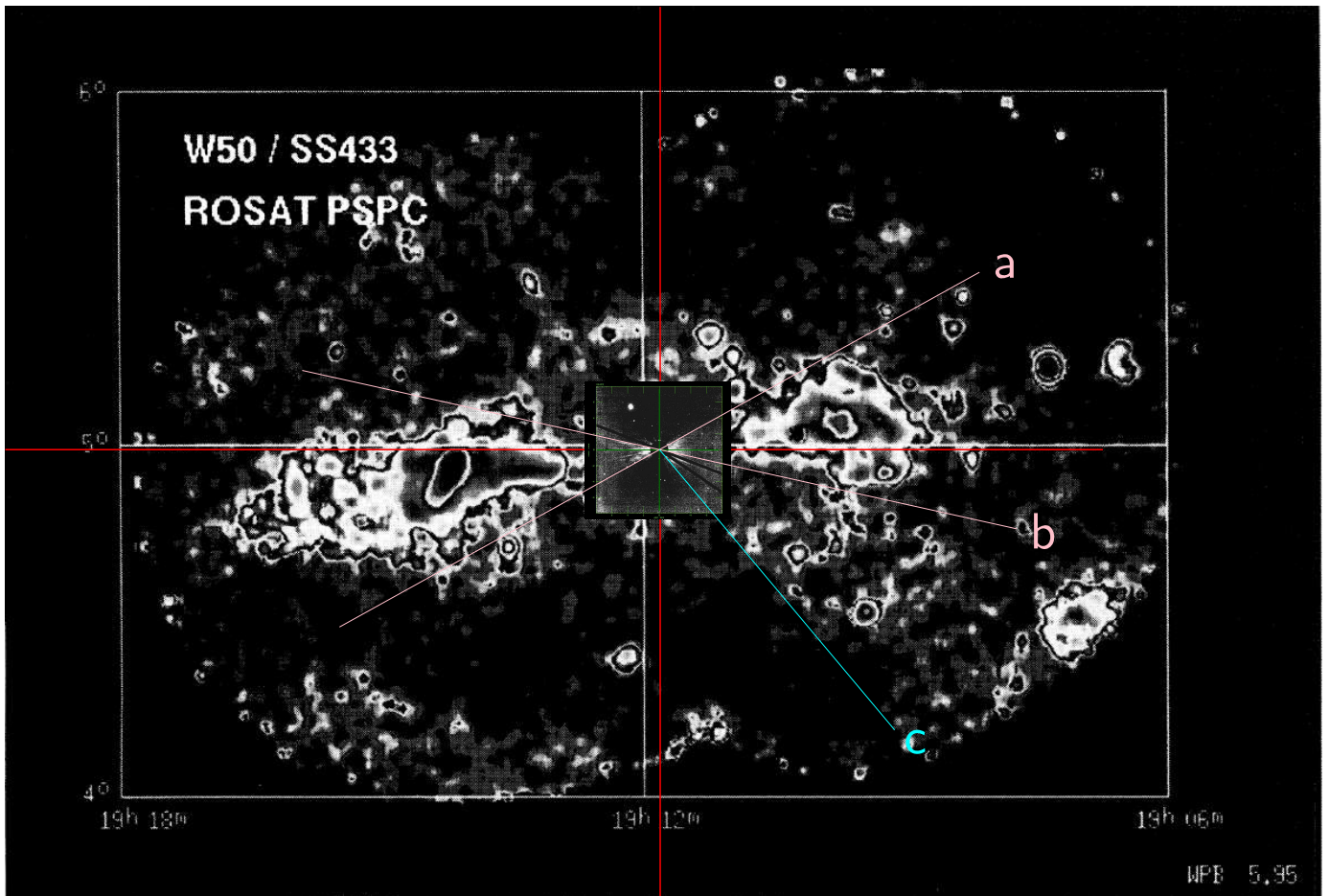


FIG. 3.— The background image is X-ray data from the ROSAT satellite (Brinkmann et al. 1996); the central inset is the same data as Figure 1, enlarged relative to the angular scale of the X-ray image. Pink lines emanate from the central inset that are matched to the edges of the eastern part of the infra-red bow tie, extended to the western side of the image. It is interesting to note that the bulk of the X-ray emission lies centrally within the pink cones. On the western side we plot in cyan a line following the southern edge of the western infra-red bow tie. It is intriguing that this line appears to mark the edge of the extended X-ray emission on the lower western side.

major outburst or flare and expelled significant quantities of material, and after sufficient time has elapsed (7 – 10 months) for the material to be propelled outwards by jet material in its precessing launch directions.

##### 5. RELATION TO OTHER STRUCTURES & CONCLUDING REMARKS

The much larger bow-tie structure observed with ROSAT by Brinkmann et al. (1996) overlaid in Fig 3 is most likely the accumulation of lots of major flare output propelled by the mechanism described in Sec 4. Note that the ROSAT bow tie is distinctly different in morphology and smaller than the 100-pc east-west extent of the W50 conch imaged at radio wavelengths (Dubner et al. 1998). The outermost regions of the W50 radio structure are believed to be caused directly by the interaction of the radio jets with the supernova remnant seen in the same radio image. Line emission takes place within hours of the jet bolides being launched from the vicinity of the black hole and then fades rapidly on a timescale of at most a couple of days (from X-ray spectroscopy (Marshall et al. 2008), optical spectroscopy (Blundell, Bowler & Schmidtobreick 2007) and near-IR spectroscopy (Perez & Blundell 2009)). It is this rapid fading of the line emission shortly after launch that ad-

ditionally rules out “normal” jet emission (i.e. intrinsic to the jet bolides, as observed by many authors within a day or so of launch) as an explanation for the infra-red bow tie shown Fig 1. The infra-red emission most likely arises as line emission from gas heated by the collision of the expanding bolides with one another as they propagate away from their launch site, propelling any gas from the vicinity of the accretion disc that intercepts the path of the wandering, precessing jet axis. These results show that the ability to observe transient behaviour in evolving microquasars can reveal entirely unexpected astrophysical behaviour. The serendipitous discovery of this transient structure is a reminder that the effect of jets of their surroundings can be considerably more dramatic than observed in steady state.

We thank ESO for the award of DDT-281.D-5062. We warmly thank Stephen Justham, Robert Laing, Stephen Blundell, Samuel Doolin, Paul Goodall and Sebastian Perez for helpful discussions. K.B. thanks the Royal Society for a University Research Fellowship. P.H. is supported by the Gemini Observatory, which is operated by the Association of Universities for Research in Astronomy, Inc., on behalf of the international Gemini partner-

ship of Argentina, Australia, Brazil, Canada, Chile, the United Kingdom, and the United States of America. The

referee is gratefully acknowledged for useful comments on the manuscript.

## REFERENCES

- Begelman, M. C., Blandford, R. D., & Rees, M. J. 1984, *Rev Mod Phys*, 56, 255
- Blundell, K. M., & Bowler, M. G. 2004, *ApJ*, 616, L159
- Blundell, K. M., & Bowler, M. G. 2005, *ApJ*, 622, L129
- Blundell, K. M., Bowler, M. G. and Schmidtobreick, L. 2007 *A&A*, 474, 903
- Blundell, K. M., Bowler, M. G., & Schmidtobreick, L. 2008, *ApJ*, 678, L47
- Blundell, K. M., Schmidtobreick L., Trushkin S., 2011, accepted by MNRAS and on arXiv.
- Bower, R. G., McCarthy, I. G., & Benson, A. J. 2008, *MNRAS*, 390, 1399
- Brinkmann, W., Aschenbach, B., & Kawai, N. 1996, *A&A*, 312, 306
- Cavaliere, A., & Lapi, A. 2008, *ApJ*, 673, L5
- Cooke, R., Bland-Hawthorn, J., Sharp, R., & Kuncic, Z. 2008, *ApJ*, 687, L29
- Dubner, G. M., Holdaway, M., Goss, W. M., & Mirabel, I. F. 1998, *AJ*, 116, 1842
- Georganopoulos, M., & Kazanas, D. 2004, *ApJ*, 604, L81
- Gladysz, S., & Christou, J. C. 2009, *ApJ*, 698, 28
- Goodall, P. T., Alouani-Bibi, F., & Blundell, K. M. 2011, *MNRAS* in press, arXiv:1101.3486
- Hjellming, R. M., & Johnston, K. J. 1981, *ApJ*, 246, L141
- Junor, W., Biretta, J. A., & Livio, M. 1999, *Nature*, 401, 891
- King, A. R. 2010, *MNRAS*, 402, 1516
- Kuncic, Z., & Bicknell, G. V. 2007, *Ap&SS*, 311, 127
- Lagrange, A.-M., et al. 2009, *A&A*, 506, 927
- Laing, R. A., & Bridle, A. H. 2004, *MNRAS*, 348, 1459
- Lenzen, R., et al. 2003, *Proc. SPIE*, 4841, 944
- Lockman, F. J., Blundell, K. M., & Goss, W. M. 2007, *MNRAS*, 381, 881
- Marshall, H. L., Canizares, C. R., Schulz, N. S., Heinz, S., Hillwig, T. C., & Mioduszewski, A. J. 2008, *International Journal of Modern Physics D*, 17, 1925
- Mioduszewski, A. J., Rupen, M. P., Walker, R. C., Schillemat, K. M., & Taylor, G. B. 2004, *Bulletin of the American Astronomical Society*, 36, 967
- Mirabel, I. F., & Rodríguez, L. F. 1999, *ARA&A*, 37, 409
- Panferov, A. A., & Fabrika, S. N. 1997, *Astronomy Reports*, 41, 506
- Perez, S., & Blundell, K. M. 2009, *MNRAS*, 397, 849
- Perez, S., & Blundell, K. M. 2010, *MNRAS*, 408, 2
- Rousset, G., et al. 2003, *Proc. SPIE*, 4839, 140